Jestr

Journal of Engineering Science and Technology Review 17 (2) (2024) 119 - 127

Research Article

JOURNAL OF
Engineering Science and Technology Review

www.jestr.org

Microcementation Mechanism of Sandy Loess Reinforced with a Cellulose Curing Agent

Dan Zhao[1], Jian Yang[1], Zhentao Liu[2], Chao Fang[2] and Rui Gao[3, 4, *]

[1]*Shangluo Highway Bureau, Shangluo, 726000, China*
[2]*Shangluo Highway Administration Bureau Asphalt Plant, Shangluo, 726000,China*
[3]*College of Architecture and Civil Engineering, Xi'an University of Science and Technology, Xi'an, 710054, China*
[4]*Road Engineering Research Center, Xi'an University of Science and Technology, Xi'an, 710054, China*

Received 9 January 2024; Accepted 31 March 2024

Abstract

Compared with typical and clay loess, sandy loess has a higher sand content and poor geotechnical engineering properties, and it easily causes geological disasters. Sandy loess reinforced with a mixture of sodium carboxymethylcellulose (CMC) + polyacrylamide (PAM) was proposed to improve the structural stability of sandy loess and reveal the curing mechanism of cellulose curing agents. The variations in the shear strength of sandy loess before and after reinforcement were analyzed through a direct shear test. The effects of the concentration of the CMC + PAM curing agent on the shear strength of sandy loess were examined. Subsequently, the soil mass before and after the reinforcement were analyzed through scanning electron microscopy, energy-dispersive spectrometry, Fourier transform infrared spectroscopy, and X-ray diffraction to reveal the micromechanism of sandy loess reinforced by the CMC + PAM curing agent. Results showed that with the increase in curing agent concentration, the shear strength of sandy loess increased considerably and gradually stabilized. When the CMC + PAM curing agent was added to natural sandy loess, the abundant hydrophilic groups in CMC and PAM bonded and adsorbed the sand particles in the soil through intermolecular forces. Large aggregates were formed after compact inlaying in the face-to-face contact mode. The porosity of sandy loess decreased, and its structural stability improved. These research conclusions can provide theoretical references for sandy loess reinforcement by cellulose curing agents.

Keywords: Sandy loess, CMC, PAM, Curing mechanism, Shear strength aggregate, Cementation

1. Introduction

Loess is a special soil with extensive distributions in arid and semiarid regions. It usually borders on deserts because of eolation, and the sand content of transition-region loess is high, thus forming sandy loess. Sandy loess has loose and porous structures, poor geotechnical engineering properties, and strong water sensitivity and water absorption. A reasonable, effective, economic and environment-friendly curing mode has been proposed to improve the geotechnical engineering properties of sandy loess and guarantee the safe construction of projects in sandy-loess regions. The structural strength and water stability of sandy loess need to be improved.

Compared with ordinary loess, sandy loess has poorer geotechnical engineering properties because of its loose and porous structures. Extant research has focused on the selection of curing agents. Traditional curing agents include cement, lime, fly ash, and asphalt materials. Untraditional curing agents include liquid polymers, enzymes, resins, acids, silicates, ions, and lignin derivatives [1-3]. Studies have demonstrated that loess reinforcement by traditional curing agents, such as cement and lime, can be divided into four processes: ion exchange, crystal hardening, pozzolanic reaction, and nitrification reaction [4]. Loess reinforced by coal ash produces calcium silicate hydrate and calcium aluminum silicate hydrate binding materials through the hydration reaction to fill in the spaces among soil particles [5]. Untraditional curing agents, such as enzymes, produce calcium carbonate through microbial induction for distribution in soils and for the bonding of loess particles, thus filling the spaces among soil particles [6]. As a derivative of lignin, calcium lignosulphonate changes the soil structure and improves soil strength mainly through cementation, filling, and agglomeration [7]. The curing mechanisms and curing effects of different curing agents vary considerably.

Sandy loess needs to be solidified using a cellulose curing agent to explain the curing mechanism of the cellulose curing agent, and the curing effect and microcementation mechanism need to be investigated. In this study, a new curing agent was prepared using a mixture of carboxymethylcellulose (CMC) and polyacrylamide (PAM) for the chemical curing of sandy loess. The mechanical properties and microcementation mechanism of the CMC+PAM curing agent were discussed.

2. State of the art

Sandy loess has loose structures, high porosity, vertical joint development, and strong collapsibility. In sandy loess, differential settlement, local wetting-induced collapse, and other phenomena easily occur under the action of external loads, such as floods and earthquakes, thus influencing building safety seriously. Many scholars have studied the macromechanical properties and microcementation

*E-mail address: 1176701374@qq.com
ISSN: 1791-2377
doi:10.25103/jestr.172.13

mechanism of sandy loess before and after solidification by curing agents and have elaborated the microcementation mechanism of curing agent-reinforced sandy loess. However, these scholars focused on the macromechanical properties of sandy loess before and after curing [8-11]. Sarli et al. [12] prepared a new curing agent by combining recycled polyester fiber and nano-SiO_2 and investigated its performance in improving the geotechnical properties of loess. The results show that the maximum dry density of cured loess decreases when the new curing agent is used, and the optimal moisture content and shear strength increase. Tabarsa et al. [13] cured loess with nanoclay and evaluated the loess curing effect of nanoclay by using the Atterberg limit, standard Proctor compaction, unconfined compressive strength, and other indexes. The results show that nanoclay influences the dispersibility and relative wetting-induced collapse behaviors of natural loess, and 2% nanoclay can improve the mechanical properties of loess remarkably. Li et al. [14] chose a liquid curing agent for roads and prepared different mixtures with lime and cement for loess modification. The results show that the resistance to compression and shear strength of sandy loess increase considerably after modification. With the increase in the curing period, the mechanical properties of modified loess develop toward hard brittleness. Nasiri et al. [15] mixed rice husk ash, lime, and soil and found that with the increase in rice husk ash, the maximum dry density of soil mass decreases, and the optimal moisture content increases. The changes in the geotechnical properties of soil are fundamentally attributed to changes in the microstructure. The aforementioned studies focused on the macromechanical properties of cured soil and paid little attention to the variation laws of the microstructure of cured loess.

Many scholars have further examined the microstructural variation laws of loess before and after curing. Ahmad et al. [16] studied the microstructure of loess by using scanning electron microscopy (SEM) and analyzed the climatic conditions corresponding to different loess strata through macroscopic observation. Ouasslia et al. [17] cured soils with wetting-induced collapse in arid regions by employing different dosages of a sodium silicate solution and revealed the microstructural changes before and after curing through SEM. Latifi et al. [2] studied the curing mechanism of a calcium-based SH-85 curing agent stabilized by red clay. Yawei et al. [18] analyzed the mineral composition and micropore structure of loess cured with quick lime in different curing ages and under different lime contents. The results show that because the hydration and volcanic ash products increase, the clay mineral content of cured soil and the number of large pores decrease; moreover, the soil structure changes to a network structure composed of acicular crystals and cement. In these studies, the curing mechanism of traditional curing agents, such as cement and lime, was investigated thoroughly. However, the chemical molecular structures of cellulose curing agents differ considerably from those of traditional curing agents, such as cement and lime. As a result, the research on the microcementation mechanism of traditional curing agents cannot serve as a theoretical reference for studying the curing mechanism of cellulose curing agents.

To explore the microcementation mechanism of loess, some scholars collected loess samples from different positions for X-ray CT scanning and found that most sand particles are flat, whereas clay particles are approximately spherical [19]. Alazigha et al. [20] performed energy-dispersive spectroscopy (EDS) to investigate a soil mass sample before and after curing with calcium lignosulphonate. They found that only some elements change slightly after curing. This finding demonstrates that intermolecular interaction, rather than chemical reaction, plays the dominant role in the relationship between soil minerals and calcium lignosulphonate. Meysam et al. [21] induced carbonate precipitation by microorganisms to improve the shear strength of sandy soils. They found from SEM images that $CaCO_3$ crystals are present in the spaces between soil sample particles after microbial-induced calcite precipitation treatment. Wu et al. [22] added different masses of sodium CMC to soils and found that CMC combines soil particles and cement bodies through cementation and friction, forming a frame structure in soils and thereby improving the mechanical properties (e.g., compression resistance and shear strength) of soils. These studies conducted a microstructural analysis of soil mass before and after curing through SEM and X-ray diffraction (XRD) and found that the curing mechanism varies in different curing modes. Determining the microcementation mechanism of sandy loess on the basis of cellulose curing agents is difficult.

A few studies have been conducted on the microstructural variation laws of loess before and after curing and found that the curing mechanisms vary in different curing agents and curing modes. To address these problems, the current study cured sandy loess with a CMC+PAM mixture to improve the physical and mechanical properties of sandy loess. The differences in surface morphology, element compositions and contents, functional groups, and chemical bonds before and after curing were discussed through SEM, EDS, and infrared spectroscopy (Fourier transform infrared or FTIR). The curing mechanisms of sandy loess after CMC+PAM curing were revealed. The research results can provide a theoretical reference for the application of cellulose curing agents in sandy loess curing.

The remainder of this study is organized into sections. Section 3 introduces the test materials, sample preparation methods, and microtest methods. Section 4 presents the direct shear test, SEM, EDS, and FTIR results of sandy loess before and after curing under different curing agent contents. The effects of curing agent types and contents on the macromechanical properties of sandy loess are discussed, and the microcementation mechanism of the curing agent in sandy loess is investigated. Section 5 provides the conclusions.

3. Methodology

3.1 Testing material

3.1.1 Cellulose curing agent

CMC is a macromolecular organic component and a carboxymethylated derivative of cellulose. It is a white powder, and its chemical formula is $[C_6H_7O_2(OH)_2OCH_2COONa]_n$, as shown in Fig. 1(a). CMC hydrogel has good cementation and water retention capabilities. However, CMC hydrogel has limited hydrogen bonds and Van Der Waals' force because of its low molecular weight. Compared with CMC, PAM has a higher molecular weight (reaching tens of millions), and it contains hard vitric crystal particles at room temperature, as shown in Fig. 1(b). PAM has good thermostability and can be dissolved in water at any ratio, and its dissolution rate in

water is higher than that of CMC. This aqueous solution is transparent and flocculent-colloidal and has stronger viscidity and cementing capacity than CMC. The two cellulose curing agents contain abundant carboxyls and hydroxyls, and they have good bonding, cementation, reinforcement, and water retention. In this study, a new cellulose curing agent was prepared by combining CMC and PAM, and the new agent's mechanical properties and cementation mechanism were explored.

(a) (b)

Fig. 1. CMC and PAM. (a) CMC. (b) PAM

3.1.2 Sandy loess

Test soil samples were collected from Luochuan County, Yan'an City, Shaanxi Province, China. The natural loess in the study area has high porosity (40%–54%) and a large pore space, and it is easily eroded by rainwater. The particle grading curve is shown in Fig. 2. The mass fraction of particles with a size larger than 100μm was large. This feature demonstrates that the soil contained abundant sand particles, and the local soil belonged to a typical sandy loess slope.

The basic physical properties of sandy loess are listed in Table 1. The natural moisture content and liquid limit of sandy loess are high, resulting in poor adhesion among soil particles and low deformation resistance. Sandy loess slopes easily cause landslides, mud–rock flow, and other disasters. Hence, sandy loess reinforcement with cellulose curing agents has theoretical and engineering value.

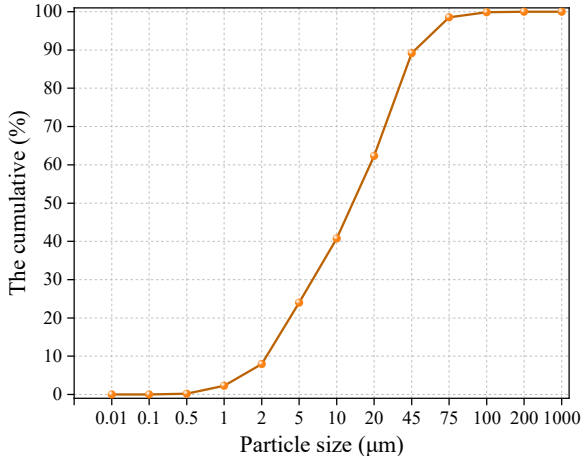

Fig. 2. Grading curve of sandy loess

3.2 Sample preparation

The collected soil samples were screened to remove gravel, roots, and other impurities and dried in an oven at 105 ℃ until a constant weight was reached. The soil samples were crushed and sieved with a 2 mm sieve. CMC and PAM solutions with different concentrations and a CMC+PAM mixture were prepared. The contents of the curing agents are shown in Table 2. The screened sandy loess and curing agent solution were mixed evenly at a liquid–solid mass ratio of 1:4 and labeled afterward. They were placed in closed containers and kept static for 24 h for subsequent tests.

Table 1. Basic physical indexes of sandy loess

Soil sample	Natural water content (%)	Soil natural density (g·cm^{-3})	Optimum water content (%)	Maximum dry density (g·cm^{-3})	Liquid limit (%)	Plastic limit (%)
Sandy loess	17.15	1.34	17.54	1.4	32.8	22.2

Table 2. Mixing ratios of the curing agents

Curing agents	Percentage concentration curing agents (%)					
CMC	0.6	1.2	1.8	2.4	3	3.6
PAM	0.6	1.2	1.8	2.4	3	3.6
CMC+PAM	0.3+0.3	0.6+0.6	0.9+0.9	1.2+1.2	1.2+1.8	1.2+2.4

3.3 Test method and equipment

3.3.1 Direct shear test

Additional stresses, including shear stress, are produced in soil mass through the action of external stresses. Soil mass exhibits shear failure when shear stress reaches a certain value. Cohesive force is produced by the mutual attraction of soil particles, and it is unrelated to external force. The internal friction angle is the sliding friction used to overcome uneven soil particle surfaces when the internal particles of soil mass slide mutually.

In this study, the shear strength of the soil samples was measured through a quick shear test under the direct shear test. A strain control-type direct shear apparatus was applied. The soil samples were placed in cylinders with a height of 20 mm and a sectional diameter of 61.8 mm. The vertical pressure was 100 kPa. The shear stress of the samples was calculated as:

$$\tau = \frac{CR}{A_0} \times 10 \quad (1)$$

where τ is shear stress (kPa), C is the calibration coefficient of the dynamometer (N/0.01 mm), R refers to the reads of the dynamometer (0.01 mm), A_0 is the sectional area of the samples, and 10 is the unit conversion coefficient.

3.3.2 Scanning electron microscopy

A SEM device is mainly composed of a vacuum system, an electron beam system, and an imaging system. The working principle of SEM is as follows. During sample scanning, electron beams are produced in the device. When the electron beams and sample surfaces interact, the sample surfaces produce secondary electrons, which present images on the screen after several transformations.

In the current test, the JSM-5600LV low-vacuum SEM device (manufactured by Electronic Optics Corporation, Japan, and Oxford Instruments, the UK) with a resolution of

3.5 nm was applied (Fig. 3). It can observe the morphologies of various substances.

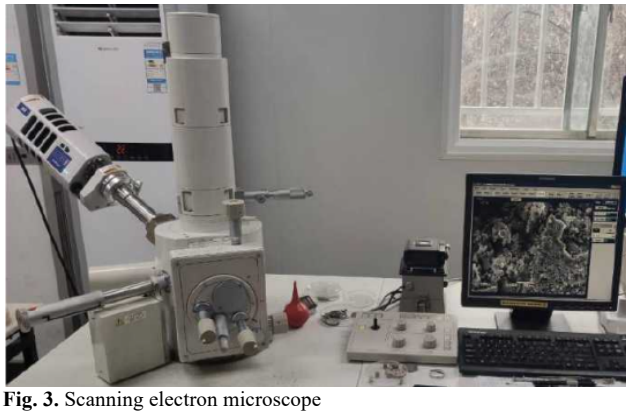

Fig. 3. Scanning electron microscope

3.3.3 Energy-dispersive spectrometry

EDS is a method to analyze object surface elements, and it is usually applied with SEM. Through EDS of sandy loess cured with different curing agent contents, a contrast analysis of the element contents of sandy loess before and after curing was performed. The MAX 80 energy-dispersive spectrometer (Oxford Instruments, the UK; Fig. 4) was used for EDS analysis of sandy loess before and after curing.

Fig. 4. Energy dispersive spectrometer

3.3.4 Fourier transform infrared spectroscopy

FTIR analyzes and identifies material molecules on the basis of infrared spectra. In this study, the differences in chemical bonds and functional groups were compared through FTIR analysis of sandy loess samples cured with different curing agent contents, and the curing mechanism of cured sandy loess was analyzed. The Bruker Tensor II Fourier infrared spectrometer was used (Fig. 5). The voltage, resolution, and scanning range were set to 220 V, 4 cm^{-1}, and 400 cm^{-1}–3,500 cm^{-1}, respectively.

Fig. 5. Fourier transform infrared spectrometer

3.3.5 X-ray diffraction

XRD investigates the crystal structures of materials and their variation laws. In this study, the differences in mineral components were investigated through XRD analysis of sandy loess samples cured with different curing agent contents. The curing mechanism of cured sandy loess was analyzed from the perspective of mineral phases. In the test, the Rigaku Ultima IV X-ray diffractometer (Fig. 6) was utilized. Cu-Kα radiation was applied, and the pipe pressure, pipe current, and scanning range were 40 kV, 40 mA, and 0°–70°, respectively. The test results were analyzed with the MDI Jade 6.0 software.

Fig. 6. X-ray diffractometer

4. Result analysis and discussion

4.1 Shear strength of the sandy loess curing bodies

The shear strength of sandy loess can reflect the resistance of a slope soil mass to external stress-induced shear deformation and rainwater erosion. The shear strength of sandy loess curing bodies can be obtained from a direct shear test and used to reveal the curing effect of sandy loess with different types and concentrations of curing agents.

The relationships between curing agent concentration and the shear strength of three cured soil samples are shown in Fig. 7. At the same liquid–solid ratio, normal pressure, and curing agent content, the shear strength of sandy loess reinforced by the CMC+PAM mixture was higher than that of sandy loess reinforced by a single curing agent. When the concentration of CMC alone was 1.2%, the shear strength of the sandy loess curing body reached the maximum then decreased gradually with the increase in curing agent concentration. When the CMC concentration exceeded 3, the CMC powder content was too high to be dissolved fully. Therefore, the shear strength of the soils cured by high-concentration CMC was not tested anymore. When PAM alone was used for reinforcement, the shear strength of the sandy loess curing body increased with the increase in PAM concentration, but it remained constant when the PAM concentration exceeded 3.6%. When the CMC+PAM mixture was applied for reinforcement, shear strength exhibited staged growth with the increase in the CMC+PAM mixture's concentration, and it increased considerably when the CMC+PAM mixture's concentration ranged from 0% to 1.8%. When the CMC+PAM mixture's concentration was 1.8% – 3%, shear strength increased slightly. Shear strength increased sharply when the CMC+PAM mixture's concentration exceeded 3%, but it remained constant when the CMC+PAM mixture's concentration exceeded 3.6%.

Under this circumstance, shear strength reached its peak, indicating an optimal curing effect.

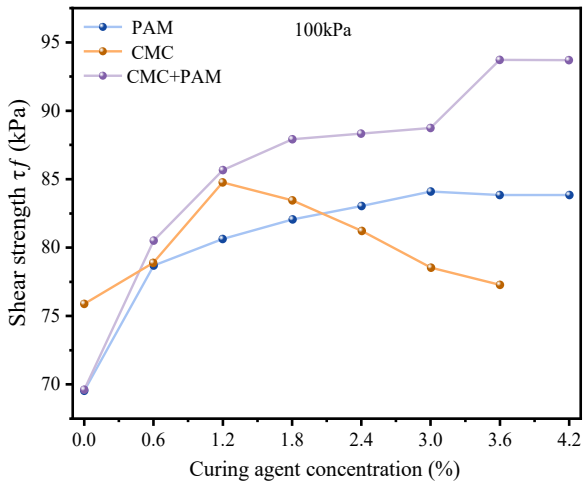

Fig. 7. Curve of the relation between curing agent concentration and shear strength

The curve of the relation between curing agent concentration and the shear strength of soils reinforced with the CMC+PAM mixture is shown in Fig. 8. At the same liquid–solid ratio and concentration, the cohesive force (c) and internal friction angle (φ) of the soils reinforced with the CMC+PAM mixture were positively related with curing agent concentration. In particular, c increased remarkably. It increased from 22 kPa for the soils without a curing agent to 38.22 kPa, indicating an increment of 16.22 kPa. Meanwhile, φ increased by only 2.1°. With the increase in the CMC+PAM mixture's concentration, c and φ increased, and shear strength increased gradually.

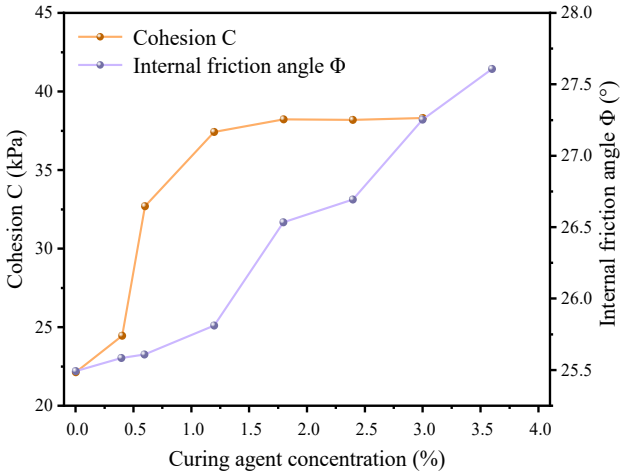

Fig. 8. Curve of the relation between CMC+PAM mixture concentration and shear strength

4.2 SEM analysis

The sandy loess curing samples with different curing agent concentrations were scanned by SEM. The curing degree and effects were compared by observing the 2D microstructures of the sandy loess curing samples, and the samples' structural stability and erosion resistance were determined.

The microstructures of natural and cured sandy loess are shown in Fig. 9. Specifically, the microstructure of natural sandy loess is shown in Fig. 9(a). When the magnification factor was 1,000, many large pores with clear overall contours were observed in the natural sandy loess. The average sand particle size in the natural sandy loess was 1 mm – 2 mm, and weak cementation structures accompanied with uneven and irregular particle distributions were found among the local soil particles. Most pores were irregular open voids with large particles and filled with sublevel sand and powder particles. Weak connections were found among the particles. Water may have infiltrated the soil pores, so the hydrophilic clay particles became soft and weak, thus destroying the internal structure of the soil mass and causing wetting-induced settlement of the surface soil particles. Accordingly, the mechanical strength of the original sandy loess declined, rainwater erosion resistance decreased, and slope stability deteriorated.

SEM images of the 1.2% CMC, 3.6% PAM, and 1.2% CMC + 2.4% PAM samples are shown in Figs. 9(b), 9(c), and 9(d), respectively. Fig. 9(b) indicates that after 1.2% CMC was added, the pores between the sandy soil particles decreased considerably compared with those in the natural sandy loess. However, small pores that were not inlaid tightly were still observed in some places. These small pores were distributed randomly without tight middle connections and resulted in an unsatisfactory curing effect because the absorption and cementation effects of CMC were not evident due to the low concentration. Fig. 9(c) shows that after 3.6% PAM was added, the particles became tightly connected and formed large aggregates. The particles demonstrated face–face contacts, which resulted in high inlaying and cementation degrees. This phenomenon increased compaction and decreased the interparticle pores effectively. Although only a few pores existed, the stability of the cured sandy loess improved considerably compared with that of the natural sandy loess because of the full development of cementation after the increase in curing agent concentration.

Fig. 9(d) shows that after 1.2% CMC + 2.4% PAM was added, large pores were hardly seen between the soil particles. The sandy and powder particles in the soil were wrapped by large-particle soil blocks under the cementation and adsorption effects of the curing agent, and large aggregates were formed. All of the aggregates were connected tightly and had high inlaying, cementation, and compaction degrees. The curing effect of CMC+PAM was better than those of CMC and PAM. The curing layer formed by the curing agent on the soil particle surfaces could resist rainwater infiltration effectively and protect the internal frame structure of the soil mass from erosion failure. As a result, the resistance to water erosion of the sandy loess slope was enhanced.

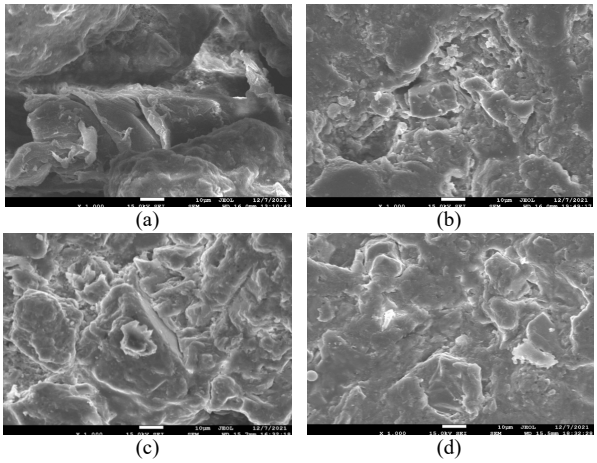

Fig. 9. SEM images of natural and cured sandy loess. (a) Natural sandy loess. (b) Soils cured with 1.2% CMC. (c) Soils cured with 3.6% PAM. (d) Soils cured with 1.2% CMC + 2.4% PAM

4.3 EDS analysis

The categories and contents of the elements in the microcell of the sandy loess curing bodies were analyzed by EDS after their microstructures were observed via SEM.

The mass proportions of the elements of the sandy loess curing bodies obtained via EDS spectral analysis are listed in Table 3. C had the maximum variance (0.29), indicating that the test value of C is slightly higher than the practical value because of the X-ray emitted from the electron scattering of C in the conductive paper pasted onto the bottom of the samples during SEM. Table 3 indicates that C, O, and Si were the major elements of natural sandy loess, and their mass proportion accounted for over 85%. This result was obtained because SiO_2 is the major mineral component of sandy loess.

Table 3. Mass proportions of the elements in cured sandy loess

Elements	wt%	wt% Sigma
C	36.03	0.29
O	37.95	0.22
H	3.22	0.05
Na	0.63	0.04
Mg	1.23	0.03
Si	15.58	0.10
K	1.14	0.04
Ca	4.51	0.06
Fe	2.92	0.10
Total	100.00	0.93

4.4 FTIR analysis

The substances and materials of the sandy loess and curing agents were analyzed and identified using infrared spectra. The organic functional groups of the substances were tested quantitatively by molecular vibrational spectra. The chemical bonds of the molecules of the sandy loess and curing agents were also investigated.

The FTIR spectra of natural sandy loess are shown in Fig. 10. The *x* axis is the spectral wavenumber that indicates the positions of absorption peaks, and the *y* axis is the transmittance. The absorption peaks of the infrared spectra at 475 cm^{-1} and 521 cm^{-1} were caused by the bending vibration of the Si–O–Al(Mg) bond. The absorption peak at 778 cm^{-1} was due to the bending vibration of C–H bonds in aromatic hydrocarbon and was a characteristic absorption peak of quartz. The absorption peak at 1,033 cm^{-1} was attributed to the stretching vibration of Si–O bonds in silicates in sandy loess, and it had a high intensity, indicating the presence of many Si–O bonds in natural sandy loess. The strong absorption peak at 1,435 cm^{-1} was caused by the bending vibration of C–H bonds in alkane, indicating the presence of many substitutive or nonsubstitutive benzene rings in natural sandy loess. The absorption peak at 1,639 cm^{-1} was attributed to the stretching vibration of carbonyl C=O bonds in amide. The absorption peak at 3,441cm^{-1} was relatively wide and may be due to the stretching vibration of hydrogen bonds (O–H) between alcohol and phenol molecules.

The FTIR spectra of sandy loess cured with 1.2% PAM are shown in Fig. 11. The absorption peak at 690 cm^{-1} was produced by the bending vibration of O–H bonds in alcohol and phenol. The peak at 778 cm^{-1} is similar to that in Fig. 10; it was caused by the out-of-plane bending vibration of C–H bonds in the aromatic hydrocarbons of sandy loess. The peak at 469 cm^{-1} indicates the possible presence of ash in the soil samples. The absorption peak at 1,023 cm^{-1} could be attributed to the stretching vibration of C–O bonds in alcohol and R–O bonds in aromatic oxides. Meanwhile, the peak at 439 cm^{-1} was caused by the bending vibration of C–H bonds in alkane, and the peak at 3,433 cm^{-1} was due to the stretching vibration of N–H bonds in amides. The peak at 2,517 cm^{-1} was the absorption peak of the associated O–H bond in carboxylic acids. The FTIR spectra showed characteristics of sandy loess and PAM after PAM was added, but no new functional groups were produced.

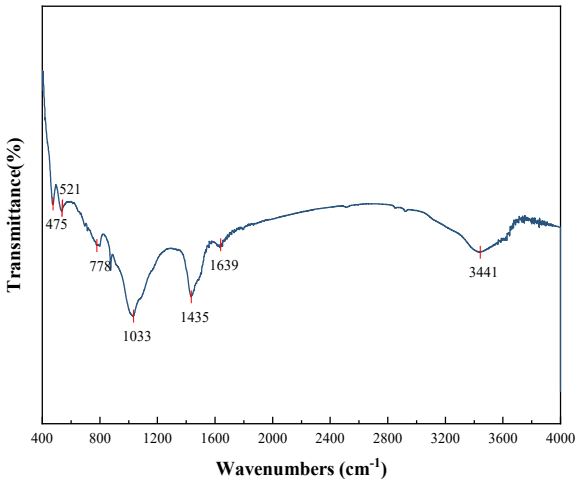

Fig. 10. FTIR spectra of natural sandy loess

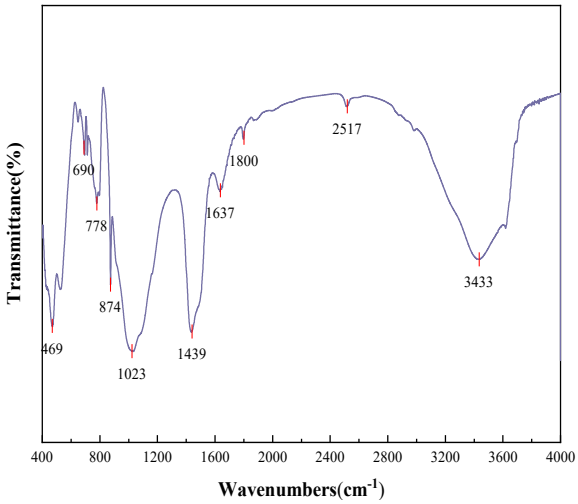

Fig. 11. FTIR spectra of sandy loess cured with 1.2% PAM

The FTIR spectra of sandy loess added with CMC and PAM at different liquid–solid ratios are shown in Fig. 12. The mass ratios of the curing agent solution and sandy loess were 0.2, 0.25, 0.3, and 0.35. Fig. 9 indicates that the FTIR spectral peaks of the sandy loess samples cured with CMC+PAM at liquid–solid ratios of 0.3 and 0.35 were consistent. The absorption peaks at 779 cm^{-1} and 777 cm^{-1} in Fig. 9 and the absorption peak at 778 cm^{-1} in Fi g. 7 were produced by the out-of-plane bending vibration of C–H bonds in the aromatic hydrocarbon of sandy loess. The absorption peaks at 1,029 cm^{-1} and 1,027 cm^{-1} corresponded to the peak at 1,023 cm^{-1} in Fig. 8, and the absorption peak at 1,638 cm^{-1} corresponded to the peak at 1,637 cm^{-1} in Fig. 8. They were caused by the stretching vibration of carbonyl C=O bonds in amides. The absorption peak at 2,520 cm^{-1} was produced by the stretching vibration of associated O–H bonds in the -COOH chain. The absorption peaks at 3,433 cm^{-1} and 3,435 cm^{-1} were due to the vibration of -NH- bonds in amides. In the sandy loess samples cured with CMC+PAM at liquid–solid ratios of 0.2 and 0.25, the characteristic peaks were not obvious because of the low

contents of CMC and PAM, and most peaks were absorption peaks of sandy loess. These results indicate that the cementation strength of the soil particles was positively related to the liquid–solid mass ratio of sandy loess cured with CMC and PAM.

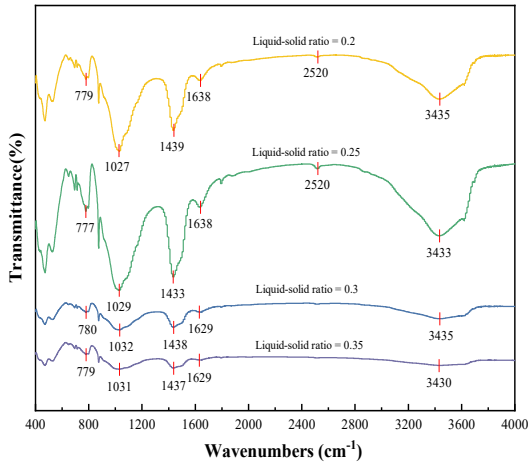

Fig. 12. FTIR spectra of sandy loess cured with CMC+PAM

The FTIR spectra of sandy loess with 1.2% CMC are shown in Fig. 13. The overall wave peak characteristics are similar to those in Fig. 10, and the similar characteristic peak is the absorption peak of natural sandy loess. The absorption peak at 3,624 cm^{-1} was caused by the stretching vibration of O–H bonds in the free hydroxyl of CMC. The absorption peak at 3,431 cm^{-1} was produced by the stretching vibration of -NH- bonds in amides. The peak at 2,882 cm^{-1} was due to the symmetric stretching vibration of C–H bonds in alkane -CH2, and the peak at 1,796 cm^{-1} was produced by the stretching vibration of C=O bonds. Meanwhile, the absorption peaks at 1,025 cm^{-1} and 1,439 cm^{-1} were offset from the FTIR spectra of natural sandy loess to some extent possibly because after CMC was added, the COO- in CMC and the original C–H bonds in sandy loess bonded. The characteristic peaks in the wavenumber range of 466 cm^{-1} – 1,025 cm^{-1} were produced by the vibrations of Si–O–Si and Si–O–Al bonds in the clay minerals (e.g., montmorillonite) in sandy loess.

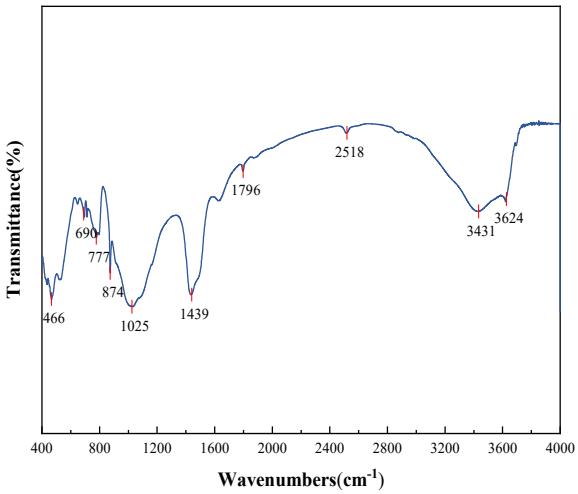

Fig. 13. FTIR spectra of sandy loess cured with 1.3% CMC

4.5 XRD analysis

The mineral elements of the cured soil bodies were tested by XRD, and the mineral components were analyzed.

The XRD spectra of the sandy loess samples with different PAM concentrations are shown in Fig. 14. According to the original data analysis via Jade software, the diffraction peak of SiO_2 was strong. SiO_2 was present when the double incidence angle (2θ) was 10°, 20°, 26.16°, 40°, and 50°, indicating that SiO_2 was the major component of sandy loess. The peak with 26° was the major characteristic peak, and the rest were secondary characteristic peaks. When 2θ = 29°, $Ca_2Al_2(SiO_3)_5$ was found, indicating the presence of anorthite. Moreover, Al_2O_3, CaO, and $Ca_3Al_2O_6$, which are products of feldspar and other silicate minerals, coexisted at about 67°.

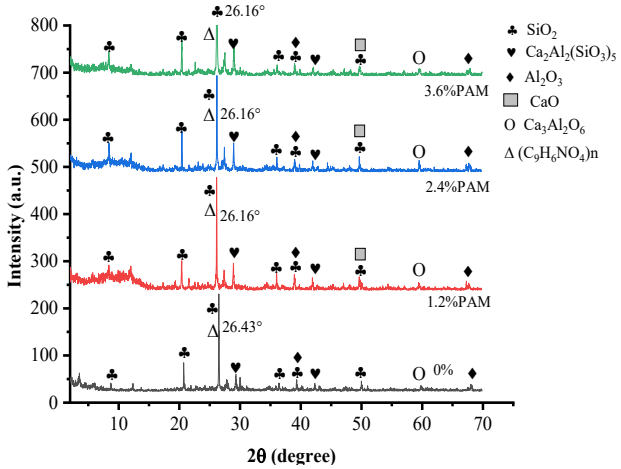

Fig. 14. XRD spectra of sandy loess samples with different PAM concentrations

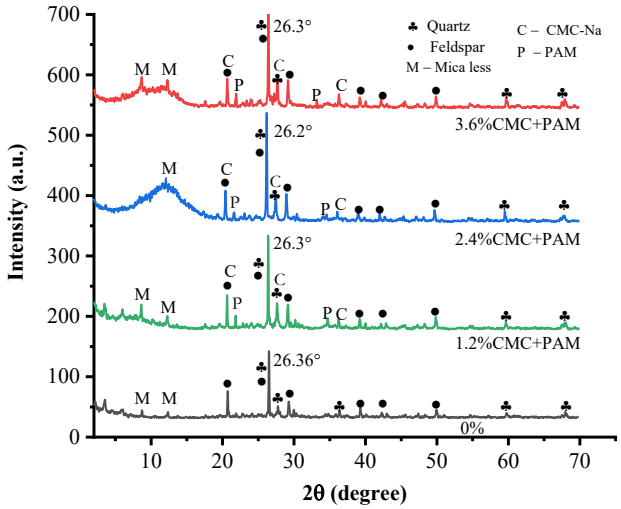

Fig. 15. XRD spectra of sandy loess cured with CMC+PAM

The XRD spectra of the sandy loess samples cured with different concentrations of the CMC+PAM mixture are shown in Fig. 15. Quartz, feldspar, and mica were the major mineral components of sandy loess. Among the components, SiO_2 had the highest content, followed by anorthite and potassium feldspar formed by compounds (e.g., calcium silicate, CaO, $Ca_3Al_2O_6$, aluminum calcium silicate, and potassium sulphate). Moreover, some aluminosilicate was formed by lamellar structures, such as K, Al, Mg, and Fe. After different concentrations of CMC and PAM were added to sandy loess, the characteristic peaks in the XRD spectra of the cured sandy loess showed elements and functional groups of CMC and PAM, including carboxyl–COOH, -OH hydroxyl-carrying hydrogen bonds, methyl-CH_3, and sodium

salt–COONa groups in CMC and methyl CH_2, acylamino–$CONH_2$, and carbonyl–C=O in PAM. These functional groups associated with Ca^{2+}, Mg^{2+}, K^+, and Si–OH ions on the particle surfaces of sandy loess through adsorption, bridging, and other physical actions of chemical bonds. As a result, the loose sandy soil particles formed compact curing layers through polymer chain jointing, resulting in soil curing. The diffraction peaks of natural and curing sandy loess were consistent, and no new diffraction peaks developed after CMC and PAM were added. This finding reveals that only physical reactions occurred after CMC and PAM were added, and no new substances were produced.

4.6 Curing mechanism analysis

The soil cementation and agglomeration induced by the CMC+PAM curing agent were mainly attributed to the abundant surface free energy in the soil particles and the molecular attractions among particles. In a series of action processes during sandy loess reinforcement by CMC and PAM, the adsorption and bonding among ions were the major reaction processes that caused various surface phenomena (Fig. 16).

After a cellulose curing agent is added to sandy loess, the groups (e.g., hydrophilic carboxyl-COOH, hydroxy-OH and methyl-CH_3) in the polymers of PAM and CMC act on the sandy soil particles through association, adsorption, bridging, and physical reactions with Si–OH, Ca^{2+}, and Mg^{2+} on their surfaces. Hence, curing layers with a certain thickness are formed on the particle surfaces. The loose sand particles and powder clays are wrapped by the acting forces among ions. The large sand particles agglomerate with the small powder particles and clays to form aggregation particles. These aggregation particles are concentrated into aggregates through adsorption. The cementation model of the aggregates of sandy loess curing bodies is shown in Fig. 16. The soil mass is connected tightly and has few pores and high cementation strength and stability because of the formation of aggregates. During rainfall, water cannot easily infiltrate the soil particles, so the infiltration rate of water is reduced, and wetting-induced settlement of sandy loess slopes is effectively prevented. Therefore, the soil mass on sandy loess slopes cannot be easily destroyed by rainwater erosion, and the effects of disasters, such as water–soil loss, collapse, landslides, and mud–rock flow, can be controlled.

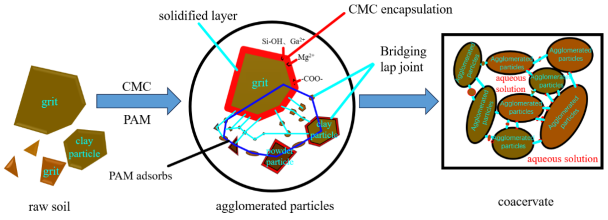

Fig. 16. Agglomeration and cementation of sandy loess reinforced with cellulose curing agent

5. Conclusion

A CMC+PAM mixture for sandy loess reinforcement was proposed in this study to investigate the curing mechanism of cellulose curing agents and improve the structural stability of sand loess. The curing effect of the CMC+PAM mixture was verified through a direct shear test from the macroscopic perspective. The changes in the microstructure and mineral composition of sandy loess before and after curing were analyzed through SEM, EDS, FTIR, and XRD. Moreover, the curing mechanisms of the CMC+PAM mixture for the reinforcement of sandy loess were discussed. The following major conclusions were obtained.

(1) The shear strength of the cured sandy loess was much higher than that of natural sandy loess. The shear strength of sandy loess cured with the CMC+PAM mixture was higher than that of sandy loess cured with CMC or PAM alone. The shear strength, cohesive force, and internal friction angle of the sandy loess curing bodies were positively related to the concentration of the curing agents. When the CMC+PAM mixture's concentration was 3.6%, the shear strength of sandy loess reached the peak and stabilized afterward.

(2) After curing, the pore diameter of sandy loess decreased, resulting in the high inlaying degree and tight bonding of the soil particles and the presence of a few large pores. The soil particles were inlaid tightly through face–face contact and had a high compaction degree. The structural stability of the soil mass was improved considerably.

(3) Quartz, feldspar, and mica were the major components of sandy loess. Among the components, O and Si had the highest content. After CMC and PAM were added, no new functional groups and chemical bonds were produced, and only physical reactions occurred. The hydrophilic groups in the curing agents formed curing layers through physical reactions (e.g., association, absorption, and bridging) with Si–OH, Ca^{2+}, and Mg^{2+} on the sandy loess surfaces, thus strengthening the structural stability of sandy loess.

The proposed CMC+PAM mixture had a good curing effect on sandy loess, and the shear strength of sandy loess improved considerably after curing. The curing mechanism of the cellulose curing agent for the reinforcement of sandy loess was revealed through microtests, such as SEM, EDS, and FTIR. This study can provide a theoretical reference for the application of cellulose curing agents in the curing of sandy loess. However, this study used only a few test groups and limited microtest data. The curing mechanism of cellulose curing agents still has to be investigated.

References

[1] A. S. A. Rashid, M. I. Shahrin, S. Horpibulsuk, M. A. Hezmi, Z. M. Yunus, and S. Borhamdin, "Development of sustainable masonry units from mud flood soil:strength and morphology investigations," *Constr. Build. Mater.*, vol. 131, pp. 682-689, Jan. 2017, doi: 10.1016/j.conbuildmat.2016.11.039.

[2] N. Latifi, A. Eisazadeh, A. Marto, and C. L. Meehan, "Tropical residual soil stabilization: a powder form material for increasing soil strength," *Constr. Build. Mater.*, vol. 147, pp. 827-836, Aug. 2017, doi:10.1016/j.conbuildmat.2017.04.115.

[3] M. Ayeldeen, A. Negm, M. El-Sawwaf, and M. Kitazume, "Enhancing mechanical behaviors of collapsible soil using two biopolymers," *J. Rock Mech. Geotech. Eng.* vol. 9, no. 1, pp. 329-339, Feb. 2017.

[4] J. Ma, "Study on mechanical properties and microscopic mechanism of oil-contaminated loess solidified by rice husk ash-lime," M. S. thesis, Dept. Archit. Civil. Eng., Lanzhou Univ. Tech., Lanzhou, China, 2022.

[5] H. Li, X. Tang, X Zhang, and M. Li, "Mechanical Properties and Microscopic Study of Steel Slag–Fly Ash-Solidified Loess under Alkaline Conditions," *Appl. Sci.*, vol. 13, no. 15, Aug. 2023, doi: 10.3390/APP13158737.

[6] Y. Ma, "Experimental study on mechanical properties and mechanism of loess reinforced by MICP technology," M. S. thesis, Dept. Mech., Taiyuan Univ. Tech., Taiyuan, China, 2021.

[7] D. Liu, Y. Zhang, X. Gao, Z. Liu, and C. Liu, "Structural mechanism of calcium lignosulfonate improved loess," (in Chinese), *J. Lanzhou. Univ. (Nat. Sci.)*, vol. 59, no. 4, pp. 468-475, Aug. 2023, doi:10.13885/j.issn.0455-2059.2023.04.006.

[8] N. F. Boaventura, T. F. D. P. Sousa, and M. D. T. Casagrande, "The Application of an Eco-Friendly Synthetic Polymer as a Sandy Soil Stabilizer," *Polym.*, vol. 15, no. 24, Dec. 2023, doi: 10.3390/POLYM15244626.

[9] N. Krzysztof, "Geotechnical Interpretation of the Geological Structure of Loess Covers in Lublin Region," *Archit. Civil Eng. Environ.*, vol. 16, no. 3, pp. 101-110, Jul. 2023, doi: 10.2478/ACEE-2023-0037.

[10] G. Magdalena, D. Marek, M. Ann, and S. Wojciech, "The origin and transformation of soil lamellae in calcareous and non-calcareous loess soils in the Central European loess belt - A case study from southern Poland," *Catena*, vol. 232, no. 2023, Nov. 2023, doi: 10.1016/J.CATENA.2023.107399.

[11] C. Dobrescu, E. Calarasu, and I. Craifaleanu, "Ground Settlement in Urban Structures Exposed to Geo-environmental and Anthropic Hazards: A Case Study for Galati," *Procedia. Eng.*, vol. 190, no. 2017, pp. 611-618, May 2017, doi: 10.1016/j.proeng.2017.05.387.

[12] J. M. Sarli, F. Hadadi, and R. Bagheri, "Stabilizing Geotechnical Properties of Loess Soil by Mixing Recycled Polyester Fiber and Nano-SiO_2," *Geotech. Geol. Eng.: Int. J.*, vol. 38, no. 8, pp. 1151-1163, Jan. 2020, doi: 10.1007/s10706-019-01078-7.

[13] A. Tabarsa, N. Latifi, C. Meehan, and K. N. Manahiloh, "Laboratory investigation and field evaluation of loess improvement using nanoclay – A sustainable material for construction," *Constr. Build. Mater.*, vol. 158, no. 2018, pp. 454-463, Jan. 2018, doi: 10.1016/j.conbuildmat.2017.09.096.

[14] H. Li, W. Zhao, and Z. Nan, "Study on mechanical properties of loess modified by Roadyes^{TM} curing agent," (in Chinese) *Chin. J. Geotech. Eng.*, vol. 45, no. S1, pp. 106-109, Nov. 2023.

[15] M. Nasiri, M. Lotfalian, A. Modarres, and W. Wu, "Optimum Utilization of Rice Husk Ash for Stabilization of Sub-base Materials in Construction and Repair Project of Forest Roads," *Croat. J. For. Eng.: J. Theor. Appl. For. Eng.*, vol. 37, no. 2, pp. 333-343, Jun. 2016.

[16] I. Ahmad and R. Chandra, "Micromorphological Study of Kashmir Loess-Paleosol Sediments: A Tool for Stratigraphic and Paleocli - matic Reconstruction," *Earth Sci. India.*, vol. 12, no. 2, pp. 83-104, Apr. 2019.

[17] B. Ouassila, T. F. Zohra, and L. Laid, "Experimental Study of the Physico-Chemical Stabilization of a Loess by Sodium Silicate: Case of Southern Algeria," *Sel. Sci. Pap. – J. Civil Eng.*, vol. 18, no. 1, Dec. 2023, doi: 10.2478/SSPJCE-2023-0013

[18] Y. Ma and W. Chen, "Study on the Mechanism of Stabilizing Loess with Lime: Analysis of Mineral and Microstructure Evolution," *Adv. Civil Eng.*, vol. 2021, no. 2021, Dec. 2021, doi: 10.1155/2021/6641496.

[19] X. Li, J. Sun, H. Ren, T. Lu, Y. Ren, and T. Pang, "The effect of particle size distribution and shape on the microscopic behaviour of loess via the DEM," *Environ. Earth Sci.*, vol. 81, no. 10, May 2022, doi: 10.1007/S12665-022-10404-X.

[20] D. P. Alazigha, B. Indraratna, J. Vinod, and A. Heitor, "Mechanisms of stabilization of expansive soil with lignosulfonate admixture," *Transp. Geotech.*, vol. 14, no. 2018, pp. 81-92, Mar. 2018, doi: 10.1016/j.trgeo.2017.11.001.

[21] B. Meysam, K. H. Ali, and M. Mohsen, "Shear Strength and Wind Erosion Potential of Biologically Improved Sand," *Geomicrobiol. J.*, vol. 38, no. 7, pp. 631-638, Sep. 2021, doi: 10.1080/01490451.2021.1917733.

[22] W. Hu, W. Cheng, S. Wen, and R. M. Mizanur, "Effects of chemical contamination on microscale structural characteristics of intact loess and resultant macroscale mechanical properties," *Catena*, vol. 203, no. 2021, Aug. 2021, doi: 10.1016/J.CATENA.2021.105361.